Energy & Environmental Science

www.rsc.org/ees

Volume 5 | Number 11 | November 2012 | Pages 9137–9674

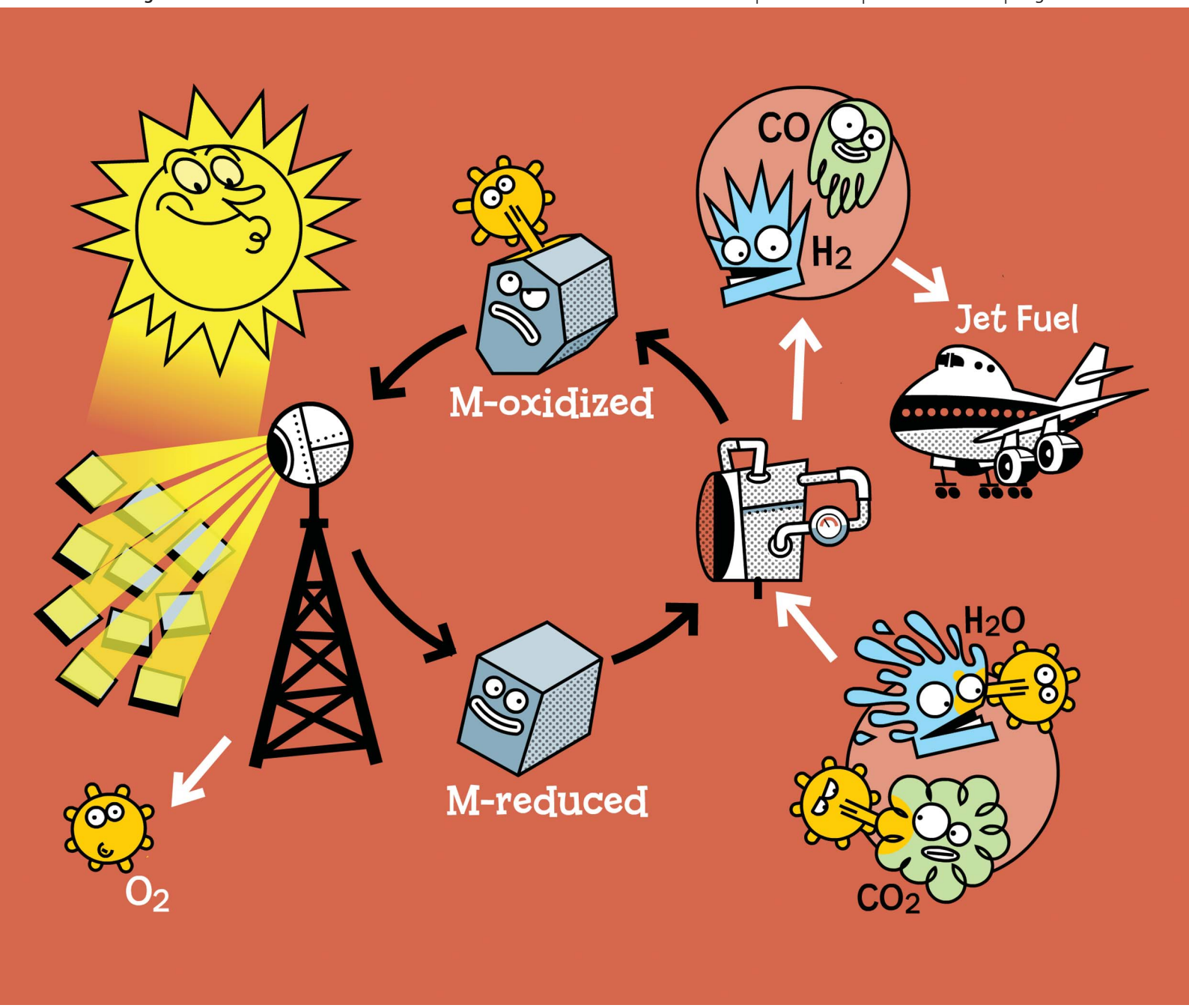

ISSN 1754-5692

RSC Publishing

REVIEW ARTICLE
Romero and Steinfeld
Concentrating solar thermal power and thermochemical fuels

1754-5692(2012)5:11;1-5

Energy & Environmental Science

Dynamic Article Links

Cite this: *Energy Environ. Sci.*, 2012, **5**, 9234

www.rsc.org/ees

REVIEW

Concentrating solar thermal power and thermochemical fuels

Manuel Romero[a] and Aldo Steinfeld*[bc]

Received 3rd February 2012, Accepted 2nd April 2012
DOI: 10.1039/c2ee21275g

Concentrated solar energy provides a virtually unlimited source of clean, non-polluting, high-temperature heat. This article reviews the underlying principles of concentrating solar radiation and describes the latest technological advances and future prospects of solar thermal power and thermochemical fuel production.

1. Introduction

For over a century devices have been designed to convert concentrated solar energy into useful work.[1–5] The oil crisis triggered R&D on solar energy and pilot plants were built during the 1980s.[6] Since 2007, the industrial implementation of concentrating solar power (CSP) is rapidly increasing, with commercial projects already totalizing several GWs. Future applications include the production of solar fuels for the transportation sector. Solar thermal and thermochemical approaches inherently operate at high temperatures and utilize the entire solar spectrum, and as such provide a thermodynamically favorable path to solar power and fuel production with high energy conversion efficiencies and, consequently, economic competitiveness.

2. Principles of solar concentration

The sun, with a solar radiosity of 63 MW m^{-2}, is an unlimited source of high-temperature heat equivalent to a 5800 K blackbody at origin. However, sun-to-earth geometrical constraints lead to a ~46 000 flux dilution to terrestrial solar irradiances of about 1 kW m^{-2}. Optical concentration devices enable high solar radiative fluxes with relatively low thermal losses.[6] They consist of large reflective surfaces collecting incident solar radiation and concentrating it onto a solar receiver.[7] The solar field is usually designed for a direct normal incident solar radiation (DNI) of 800 W m^{-2} and for an annual DNI in the range 1600–2800 kW h m^{-2}, allowing for 2000 to 3500 annual full-load solar operating hours.[8] Because CSP is restricted to DNI, the sun-belt region (±40°) is mainly considered for its application, while zones with a high degree of humidity and/or aerosols are not appropriate. CSP plants can dispatch power round-the-clock by incorporating a thermal storage system and over-sizing the solar field accordingly.

Solar concentrators follow the basic optical principles of Snell's law for reflection by specular surfaces.[9] Parabolic concentrators and their analogues are used in large-scale CSP systems because they exhibit the greatest potential for scaling up at reasonable costs. Their capability of concentration is given by the solar concentration ratio C defined as the mean solar radiative power flux over the focused area, normalized to the DNI. The maximum solar concentration ratio for an ideal perfectly specular 3-D paraboloid of rim angle ϕ_{rim} aligned to the sun is[10] $C_{max} = \sin^2 \phi_{rim}/(4\sin^2 \theta_S)$, where θ_S is the semi-angle subtended

[a]*IMDEA Energy Institute, Avda. Ramon de la Sagra, 3, 28935 Mostoles, Spain*
[b]*Department of Mechanical and Process Engineering, ETH Zurich, 8092 Zurich, Switzerland. E-mail: aldo.steinfeld@ethz.ch*
[c]*Solar Technology Laboratory, Paul Scherrer Institute, 5232 Villigen PSI, Switzerland*

Broader context

Concentrated solar radiation is used as the energy source of high-temperature process heat for the thermal production of solar power and chemical fuels. Next generation of concentrating solar power (CSP) technologies will enable superior integration of thermal storage and hybridization with fossil fuel backup for round-the-clock power dispatchability. Novel solar receiver concepts based on volumetric absorption of directly irradiated porous structures, particles, and alternative thermal fluids will operate at high temperatures (above 1000 °C) and high solar fluxes (above 2000 suns) for efficient capture and conversion of concentrated solar energy, e.g. via Brayton-Rankine combined cycles. These advanced concepts can be also applied for the thermochemical production of solar fuels. Solar thermal cracking, reforming, and gasification processes for upgrading and converting carbonaceous feedstock to transportation fuels can conserve fossil fuels, reduce CO_2 emissions, and become important transition paths towards solar fuels. The production of solar hydrogen, syngas, and liquid hydrocarbons from H_2O and CO_2 via redox thermochemical cycles has favorable long-term potential, warranting further development and large-scale demonstration.

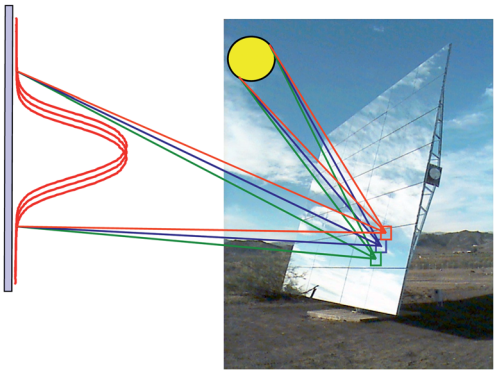

Fig. 1 The convolution of sunshape and random surface errors originates a Gaussian profile on the concentrated solar image.

by the sun, 4.653 mrad (16′). For $\phi_{rim} = 90°$, $C_{max} \approx 11\,547$. The solar concentration ratio can be augmented by non-imaging compound parabolic concentrators (CPCs[11]) in tandem with primary parabolic concentrators by a factor $C_{CPC,3D} = \sin^{-2} \phi_{CPC}$ and $C_{CPC,2D} = \sin^{-1} \phi_{CPC}$, where ϕ_{CPC} is the CPC acceptance angle. The theoretical limit is 46200 and 215 for the 3D and 2D, respectively, for $\phi_{CPC} = \theta_S$. In practice, C is significantly lower because of the sunshape, reflection losses, and surface and tracking errors. The random surface errors are either microscopic (specularity) or macroscopic (mirror waviness and curvature), and result in a Gaussian shape of reflected rays as depicted in Fig. 1, which can be fitted to a normal distribution function. Its standard deviation, commonly known as beam quality, is typically a few mrad and determines the size of the solar receiver aperture.

Four solar concentrating technologies are currently applied at pilot and commercial CSP plants,[12,13] namely parabolic trough (PT) collectors, linear Fresnel (LF) reflector systems, dish–engine (DE) systems, and power towers—also known as central receiver (CR) systems. These concentrating technologies, schematically shown in Fig. 2, mimic parabolic geometries with large mirror areas.

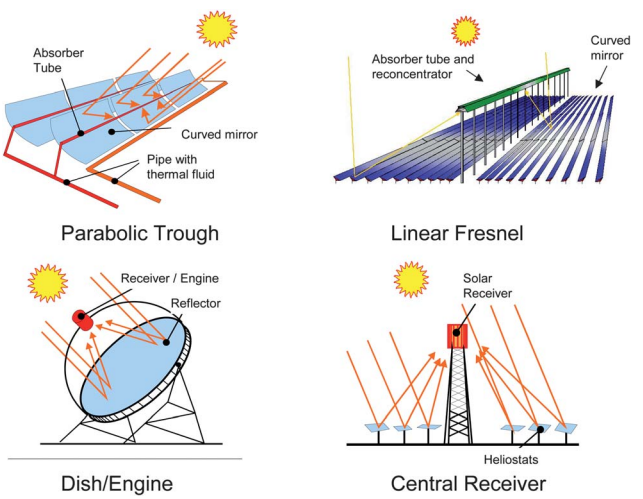

Fig. 2 Schematics the four solar concentrating technologies currently applied at commercial CSP plants: parabolic trough collectors (PT), linear Fresnel reflector systems (LF), dish–engine systems (DE), and power towers—also known as central receiver systems (CR). PT and LF are 2-D systems with linear focus; DE and CR are 3-D systems with point focus.

PT and LF are 2-D concentrating systems that focus the incident solar radiation onto a solar receiver mounted along the focal line by one-axis tracking mirrors. Typically, C ranges between 30 and 80, thermal fluid temperatures are up to 500 °C, and thermal power outputs are from 30 to 700 MW. Thus, they are well suited for centralized power generation at dispatchable markets with a Rankine steam turbine/generator cycle. CR are 3-D concentrating systems that focus the incident solar radiation onto a solar receiver mounted on top of a tower by means of a large paraboloid that is discretized into a field of two-axis tracking heliostats. Typically, C ranges between 200 and 1000, thermal fluid temperatures are above 500 °C, and thermal power outputs are from 50 to 300 MW. Thus, they are well-suited for dispatchable markets and integration into advanced thermodynamic cycles or thermochemical processes. A wide variety of thermal fluids, such as saturated or superheated steam, molten salts, and atmospheric or pressurized air, can be used in the temperature range 500–2000 °C. The Cassegrain optical configuration for CR systems makes use of a hyperboloidal reflector at the top of the tower to re-direct sunlight to a receiver located on the ground level.[14] DE are smaller 3-D two-axis tracking parabolic concentrators that focus the incident solar radiation onto a Stirling engine or Brayton mini-turbine mounted at the focal point. Typically, C ranges between 1000 and 3000. They are autonomous modules of 5–25 kW power output, with a market niche in distributed on-grid and remote/off-grid power applications.[15–18] For all four solar technologies, higher values of C can be achieved by the incorporation of non-imaging secondary concentrators, *e.g.* CPC,[11] at the solar receiver aperture.

3. Characteristics of CSP systems

Representative solar-to-electric conversion efficiencies and annual capacity factors are listed in Table 1. Note that the LF systems are not included since available performance data are not yet conclusive for a comparative assessment. The values for

Table 1 Characteristics of CSP systems

	Parabolic troughs	Central receiver	Dish/engine
Power unit	30–80 MW[a]	10–200 MW[a]	5–25 kW
Temperature operation	390 °C	565 °C	750 °C
Annual capacity factor	23–50%[a]	20–77%[a]	25%
Peak efficiency	20%	23%	29.4%
Net annual efficiency	11–16%[a]	7–20%[a]	12–25%
Commercial status	Mature	Early projects	Prototypes-demos
Technology risk	Low	Medium	High
Thermal storage	Limited	Yes	Batteries
Hybrid schemes	Yes	Yes	Yes
Cost W installed			
$ per W	3.49–2.34[a]	3.83–2.16[a]	11.00–1.14[a]
$ per Wpeak[b]	3.49–1.13[a]	2.09–0.78[a]	11.00–0.96[a]

[a] Data interval for the period 2010–2025. [b] Without thermal storage.

PT, by far the most mature technology, have been demonstrated for over two decades in established commercial projects. Those for LF, DE, and CR systems are projections based on early commercial projects and the assumption of further development. With current investment costs and market prices, all CSP systems generally require public financial incentives for market penetration, as direct capital and power generation costs of CSP are estimated to be 2–3 times those of fossil-fueled power plants. Nevertheless, industry roadmaps anticipate a 60% cost reduction of CSP by 2025.[19] Spain and other countries are already accelerating the phasing-out of feed-in tariffs with the goal of making CSP, PV, and wind energy tariff-equivalent in less than a decade.

In terms of electric grid and quality of bulk power supply, it is the ability to dispatch round-the-clock and on-demand that makes CSP stand out over other renewable technologies such as intermittent PV and wind electricity. Thermal energy storage systems store excess sensible heat collected by the solar field and, alone or in combination with fossil fuel backup, keep the plant running under full-load conditions after sunset. This storage capability leads to economically competitive design options since only the solar part is oversized, and enables penetration into the bulk electricity market where substitution of intermediate-load power plants of about 4000–5000 hours per year is achieved.

By end of 2011, Spain and the US were leading the commercialization of CSP with more than 1.5 GW in operation and more than 6 GW of projects under development.[20] India, China, Australia, Italy, and other countries with vast solar irradiation (DNI) resources have adopted the support of CSP and are considered potential future markets. A clear indicator of the globalization of CSP commercial deployment for the future energy scenario has been elaborated by the International Energy Agency,[21] which considers CSP to play a significant role among the necessary energy mix for halving global CO_2 emissions by 2050. This scenario would require the capacity addition of 14 GW annually, *i.e.* about 55 new CSP plants of 250 MW each per year.

The projected evolution of levelized electricity costs (LECs) of different CSP technologies is depicted in Fig. 3. LEC reduction is expected from mass production, scaling-up, and R&D. A technology roadmap promoted by the European Industry Association[19] indicates that by 2015 increase of efficiencies by 10% and decrease of costs by up to 20% are to be expected provided various improvements currently under development are implemented in the new generation plants. Furthermore, economies of scale resulting from plant size increase will also contribute to reduce plants' CAPEX per MW installed by up to 30%. CSP deployment in locations with very high DNI further contributes to cost reduction up to 25%. All these factors combined can lead to electricity generation cost savings of up to 30% by 2015 and up to 50% by 2025, reaching competitive levels with conventional fossil fuel sources with stabilized LEC below €0.10 per kW h. Similar projections are published in a recent roadmap issued by the IEA.[22] Other roadmaps coordinated by R&D centers predict a larger influence of innovations (up to 25%) in cost reduction.[23]

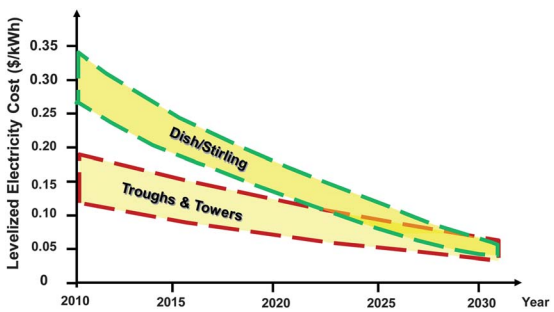

Fig. 3 Projection of levelized electricity cost for CSP technologies based upon technology roadmaps and industry.

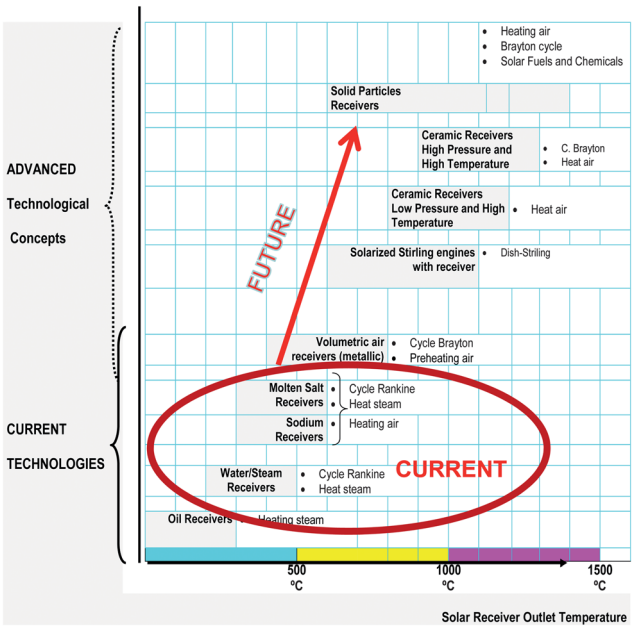

Fig. 4 Evolution of CSP. Current technologies are based on solar receivers that operate with thermal oil or water–steam at working temperatures usually below 500 °C, coupled to steam-based Rankine cycles. The next generation of technologies allows surpassing 1000 °C and enables higher efficiencies *via* Brayton and combined cycles, as well as the thermochemical production of solar fuels.

The first generation of commercial CSP projects is adopting technologies and concepts that have matured in the last 30 years. They are based on conservative designs and schemes which do not necessarily exploit the enormous potential of concentrated solar energy. Fig. 4 illustrates the situation. Current technologies are based on solar receivers operating at moderate solar concentration ratios with thermal oil or water–steam at working temperatures usually below 500 °C, which are coupled to steam-based Rankine cycles. As a consequence, solar-to-electricity conversion efficiencies are below 20%, the application of energy storage is limited, water consumption and land use are relatively high, the power block integration is rather inefficient, and the thermochemical routes to produce solar fuels are beyond reach. The next generation of CSP plants allows surpassing 1000 °C and enables higher efficiencies *via* Brayton and combined cycles as well as better integration of thermal storage. Novel receiver concepts based on volumetric absorption of directly irradiated porous structures and particles, with alternative thermal fluids (*e.g.* air), operate at higher solar concentration ratios and promise more efficient solar energy capture and conversions. Moreover, these advance concepts open the door to the thermochemical production of solar fuels. The solar concentrating

technologies better adapted for these applications are solar towers (CR), whose current development mainly for power generation is paving the way for future high flux/high temperature thermochemical applications.

Challenges and key general topics for the medium to long-term R&D are improved designs of materials and components, increased system efficiency through higher operating temperatures, high reliability during unattended operation, hybrid solar–fossil fuel plants with small solar share, and solar share increase through integration of storage.[12] R&D is multidisciplinary, involving optics, materials science, thermal engineering, and control and measurement techniques. Specifically, for PT and LF systems, R&D is aimed at lighter and lower-cost structural designs including front surface mirrors with high solar-weighted reflectivity of about 95%; high-absorptance (>96%) coatings for tube receivers able to operate at above 500 °C; medium temperature thermal energy storage systems based on phase change materials, molten salts, concrete, and packed bed of rocks suitable for solar-only systems; improvement in overall system O&M, including mirror cleaning, integral automation, and unattended control; system cost reductions and efficiency improvements by direct steam generation; and alternative heat transfer fluids such as air.[24] For CR systems, R&D is aimed at improvements in the heliostat field as a result of superior optical properties, lower cost structures, and better control; development of water–superheated steam and advanced air-cooled volumetric receivers using wire-mesh absorbers or ceramic monoliths and foams; advanced thermocline storage systems based on packed-bed of ceramic materials[25] (especially suitable for solar air-receivers) and high-temperature thermochemical storage; and distributed control architectures, system integration, and hybridization in high-efficiency electricity production schemes. For DE, R&D is aimed at volumetric receivers coupled to Stirling and Brayton engines; improvements in mirrors and support structures; and improvements in system integration and control for fully automation, parasitic loads reduction, startup optimization, and hybrid Stirling–Brayton operation.

Alternative heat-to-electricity energy conversion devices that can potentially use CSP technologies include thermoelectric,[26] magnetohydrodynamic,[27] and thermionic converters.[28] In particular, thermoelectric conversion based on the Seebeck effect becomes attractive for decentralized DE applications[29] and for recovering solar waste heat.

4. Central receiver systems: current developments and future prospects

In CR concentrating systems, incident sunrays are tracked by heliostats and focused onto the solar receiver mounted on top of a tower, where energy is transferred to a thermal fluid. Plants of power output of 10 to 200 MW_e are being deployed in early markets in US, Spain, South Africa, and others, because of economy of scale and feed-in tariffs. Advanced integration schemes are claiming the economics of smaller units as well.[30] The high C on the receiver enables operation at above 1000 °C and integration into more efficient heat engines. CR can also be integrated in conventional fossil fuel based plants for hybrid operation in a wide variety of options and has the potential for generating electricity with high annual capacity factors through the incorporation of thermal storage. With thermal storage, CR plants are able to operate over 4500 hours per year at nominal power[31] and dispatch solar electricity round-the-clock. Although there have been a large number of CR projects, only a few have culminated in the construction of the entire CSP system.[32,33] Typical thermal fluids used in the receiver are liquid sodium, saturated or superheated steam, nitrate-based molten salts, and air. Extensive pre-commercial experience has been collected by several European projects located at the Plataforma Solar de Almería[33] in Spain and by the 10 MW Solar One[34] and Solar Two[35] plants in the US. At present, water–steam and molten salts are the heat transfer fluids selected for the first generation of commercial CSP plants. Two pioneering projects, PS10 and PS20, are producing electricity from saturated steam since 2007. New projects by Abengoa Solar, Brightsource, and eSolar demonstrate the feasibility of producing superheated steam at above 500 °C with dual receivers.[12] The 17 MW_e Gemasolar plant developed by Torresol Energy,[36] connected to grid in summer 2011 (Fig. 5), uses molten salt as heat transfer fluid and for thermal storage. A circular heliostat field of 304 750 m^2, 115 m^2 each heliostat, is oversized to supply 15 hour equivalent heat storage capacity and generates 112 GW_{he} per year with an annual capacity factor of 74%. The plant is designed to operate round-the-clock in summertime.[37]

Fig. 5 Aerial view of Gemasolar CSP plant located in south of Spain, which uses CR technology with a circular heliostat field and molten salt for thermal storage (left). Lateral view of the cylindrical solar receiver containing vertical tubes with molten salt as heat transfer fluid (right). The plant is designed to operate round-the-clock in summertime. Source: Torresol Energy.

Heliostat field

The two-axis tracking heliostats have a local control unit for continuously focusing the incident solar radiation onto the receiver aperture. Heliostat fields are characterized by their off-axis optics, placing their surface normal to the bisection of the angle subtended by sun and the solar receiver, *i.e.* the "cosine" effect. The annual average cosine varies from 0.9 to 0.7, and is highly dependent on site latitude. The optical efficiency accounts for the cosine effect, shadowing, blocking, mirror reflectivity, atmospheric attenuation, and receiver spillage.[32] Because of the relatively large area of land required, ray-tracing algorithms are applied to optimize the heliostat layout and establish the radial and azimuthal spacing of heliostats and rows.[38,39] One effective procedure is the radial staggered pattern.[40,41] Close to the equator, a circular field is best to reduce land use and tower height. North/south fields improve performance as latitude increases in north/south hemispheres. Integral optimization of

the heliostat layout is decided by a tradeoff between cost and performance parameters, which often have reverse trends because of blocking and shadowing penalties as packing increases.

The historical development of heliostats shows a trend from the early first generation prototypes[42] with 40 m^2 reflecting surfaces and heavy, rigid structures, to designs with large 100–120 m^2 reflecting surfaces, lighter structures, and lower-cost materials.[43,44] 120 m^2 heliostats were finally adopted for the first commercial CR plants PS10 and PS20 developed by Abengoa Solar.[45] Beam qualities below 2.5 mrad (not including sunshape) are good enough for practical applications in solar towers, so that the main focus of development is directed at cost reduction. Estimated production costs of large area glass–metal heliostats[46] (glass mirrors supported by metallic frame facets) for sustainable market scenarios are in the range \$130–200 per m^2. The paradigm of maximum modularity and mass production led to the development of small-size heliostats as a competitive low-cost option. Brightsource uses single-facet 7.3 m^2 heliostats.[47] eSolar uses a multitower plant configuration with ganged 1.14 m^2 heliostats—12 180 units for a single 2.5 MW tower[48]—at installed costs below \$200 per m^2 because of preassembly and simpler on-site mounting.

Solar receivers

The solar receiver approaches a blackbody in its capability to trap incident solar radiation by making use of cavities, black-painted tube panels, or volumetric porous absorbers. In most designs, the solar receiver is a single unit that centralizes all the energy collected by the heliostat field, imposing high availability and durability. High thermal efficiency is of paramount importance as it directly impacts the size of the heliostat field and, consequently, the electricity cost. Typical receiver operating temperatures for electricity generation are in the range of 500–1200 °C for incident solar fluxes between 300 and 1000 kW m^{-2}, depending on the thermal fluid and application.[7,49] According to the geometrical configuration, there are basically two design options: external and cavity-type receivers. In a cavity-receiver, the incident concentrated solar radiation enters through a small aperture into a well-insulated enclosure containing the absorber. Cavities are constrained angularly and subsequently used in north/south-field layouts. In contrast, external receivers can be cylindrically shaped for surround heliostat fields (see Fig. 5). Receivers can be directly or indirectly irradiated.[50] Directly irradiated receivers make use of fluids or particle streams directly exposed to the concentrated solar radiation. A transparent window is required for pressurized applications. Indirectly irradiated receivers consist of absorbing surfaces exposed to the concentrated solar radiation, with heat conducted across the walls to the thermal fluid. Table 2 lists operating temperature and solar flux ranges of solar receivers for CR. It is possible to reach solar fluxes above 1 MW m^{-2} with high thermal conductivity liquids, *e.g.* sodium. Air-cooled receivers have inherently lower heat transfer coefficients. Wire meshes (knitted or layered grids), reticulated foams (metallic or ceramic), and other highly open-cell porous structures are used in directly irradiated receivers to improve the contact surface[51] and their effective heat/mass transport properties.[52] These so-called "volumetric" absorbers

Table 2 Temperature and solar flux ranges of solar receivers for CR

Fluid	Water–steam	Liquid sodium	Molten salt (nitrates)	Air (volumetric)
Solar Flux (MW m^{-2})				
Average	0.1–0.3	0.4–0.5	0.4–0.5	0.5–0.6
Peak	0.4–0.6	1.4–2.5	0.7–0.8	0.8–1.0
Fluid outlet temperature (°C)	490–525	540	540–565	700 to >1000

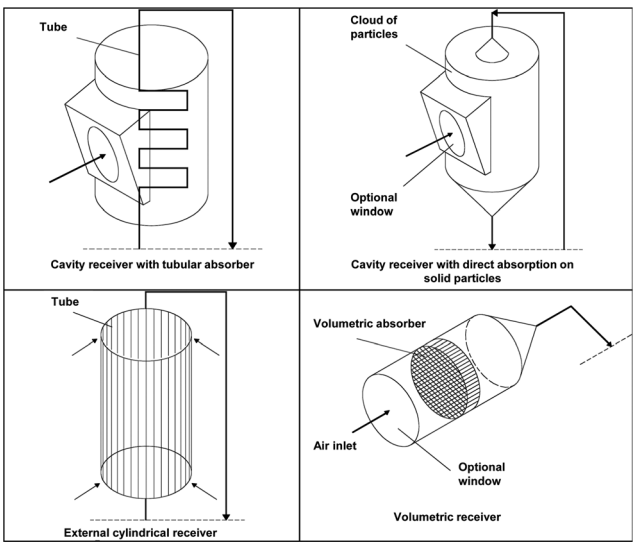

Fig. 6 Examples of solar receiver configurations: (a) cavity-receiver with tubular panel, (b) cavity-receiver with direct absorption on particle-laden flow, (c) external receiver with tubular panels and (d) volumetric receiver with porous absorber.

enable the concentrated solar radiation to penetrate and be absorbed within the volume.[53,54] To avoid unstable mass flow distribution, perforated plates are introduced behind the absorber.[55,56] Air-cooled volumetric receivers can be designed for atmospheric pressure[57,58] and for pressurized systems,[49,59,60] but their current efficiencies must be improved.[61] Fig. 6 schematically shows examples of configurations of cavity, external, and volumetric receivers. The selection of a particular receiver concept is a complex task and strongly depends on the operating temperature, heat storage, and thermodynamic cycle. Tubular receiver concepts are suitable for applications at either high temperatures (up to 1200 °C) or high pressures (up to 120 bar), but usually not both because of material constraints.[62] Conversely, directly irradiated or volumetric receivers are suitable for applications at higher temperatures but limited pressures (>15 bar) because of window constraints.

5. Thermodynamics of solar thermochemical conversion

Solar thermochemical processes make use of concentrated solar radiation as the energy source of high-temperature process heat to drive endothermic reactions.[63] Solar reactors for highly concentrated solar systems usually feature cavity-receiver configurations, *i.e.* a well-insulated enclosure with a small

aperture to let in concentrated solar radiation. Because of multiple internal reflections, the fraction of the incoming energy absorbed by the cavity greatly exceeds the surface absorptance of the inner walls. As the ratio of the cavity's characteristic length to the aperture diameter increases, the cavity-receiver approaches a blackbody absorber. The solar energy absorption efficiency of a solar cavity-receiver, $\eta_{\text{absorption}}$, is defined as the net rate at which energy is being absorbed divided by the solar radiative power coming from the solar concentrator system that is intercepted by the aperture, Q_{solar}. For a perfectly insulated cavity-receiver (no convection–conduction heat losses) operating at a nominal temperature T, it is given by:[64]

$$\eta_{\text{absorption}} = 1 - \left(\frac{\sigma T^4}{IC}\right) \quad (1)$$

where C is the mean solar flux concentration ratio over the cavity's aperture area, normalized to the DNI I. The measure of how well solar energy is converted into chemical energy for a given thermochemical process is the solar-to-fuel energy conversion efficiency, $\eta_{\text{solar-to-fuel}}$, defined as

$$\eta_{\text{solar-to-fuel}} = \frac{-\Delta G}{Q_{\text{solar}}} \quad (2)$$

where ΔG is the maximum possible amount of work that may be extracted from the products at 298 K. Note that $\eta_{\text{solar-to-fuel}}$ is sometimes reported based on ΔH instead of ΔG, *i.e.* based on the high heating value (HHV) of the fuel produced; the corresponding factor should be applied when comparing with the efficiency defined by eqn (2).The Second Law is now applied to calculate the maximum $\eta_{\text{solar-to-fuel}}$ for an ideal cyclic process, limited by both the solar absorption and Carnot efficiencies,

$$\eta_{\text{solar-to-fuel,ideal}} = \left[1 - \left(\frac{\sigma T_{\text{H}}^4}{IC}\right)\right] \times \left[1 - \left(\frac{T_{\text{L}}}{T_{\text{H}}}\right)\right] \quad (3)$$

where T_{H} and T_{L} are the upper and lower operating temperatures of the equivalent Carnot heat engine, respectively. $\eta_{\text{solar-to-fuel,ideal}}$ is plotted in Fig. 7 as a function of T_{H} for $T_{\text{L}} = 298$ K and for various solar flux concentrations. Because of the Carnot limitation, one should try to operate thermochemical processes at the highest upper temperature possible; however, from a heat-transfer perspective, higher T_{H} implies higher re-radiation losses. There is an optimum temperature T_{optimum} for maximum efficiency shown in Fig. 7, which varies between 1100 and 1800 K for uniform solar flux distributions with C between 1000 and 13 000. For example, for $C = 5000$, the maximum $\eta_{\text{solar-to-fuel,ideal}}$ of 75% is achieved at $T_{\text{optimum}} = 1500$ K. For a Gaussian incident solar flux distribution having peak concentration ratios between 1000 and 12 000 suns, the optimal temperature varies from 800 to 1300 K. In practice, when considering convection and conduction losses in addition to radiation losses, the efficiency will peak at a somewhat lower temperature. $\eta_{\text{solar-to-fuel}}$ increases with C because of the smaller aperture to intercept the same amount of solar power, and, consequently, lower re-radiation losses. Re-radiation losses can also be diminished by implementing selective windows with high transmissivity in the solar spectrum around 0.5 μm where the solar irradiation peaks, and high reflectivity in the near infrared range where the Plank's spectral emissive power for a blackbody at T peaks.

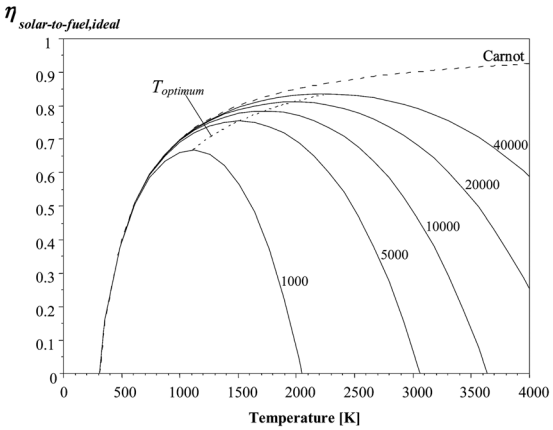

Fig. 7 Variation of the ideal solar-to-fuel energy conversion efficiency as a function of the operating temperature T_{H}, for a blackbody cavity-receiver converting concentrated solar energy into chemical energy. The mean solar flux concentration is the parameter. Indicated is T_{optimum} for maximum $\eta_{\text{solar-to-fuel,ideal}}$.[63]

Eqn (2) establishes a base for evaluating and comparing different solar thermochemical processes for ideal, closed cyclic systems. For open materials cycles, in which carbonaceous feedstocks are being solar-upgraded (see next section: cracking, reforming, gasification), the solar-to-fuel energy conversion efficiency is defined as

$$\eta_{\text{solar-to-fuel}} = \frac{-\Delta G}{Q_{\text{solar}} + \text{HHV}_{\text{reactants}}} \quad (4)$$

where $\text{HHV}_{\text{reactant}}$ is the high heating value of the feedstock being processed, *e.g.* about 890 kJ mol^{-1} for natural gas and 35 700 kJ kg^{-1} for anthracite coal. Analogous to eqn (2), $\eta_{\text{solar-to-fuel}}$ is sometimes reported based on ΔH instead of ΔG, *i.e.* based on the high heating value (HHV) of the fuel produced. The higher $\eta_{\text{solar-to-fuel}}$ the lower is the required solar collection area for producing a given amount of solar fuel and, consequently, the lower are the costs incurred for the solar concentrating system, which usually correspond to half of the total investments for the entire solar chemical plant. Thus, high $\eta_{\text{solar-to-fuel}}$ implies favorable economic competitiveness.

6. Solar thermochemical processes and reactors

Five thermochemical routes for solar fuel production are depicted in Fig. 8.[65] Indicated is the chemical feedstock: H_2O/CO_2 and/or carbonaceous feedstock (*e.g.* natural gas, oil, coal, and biomass). Based on the feedstock, the processes are grouped into H_2O/CO_2-splitting processes (thermolysis and thermochemical cycles) and decarbonization processes (cracking, reforming, and gasification). All these thermochemical routes are highly endothermic processes that proceed at high temperatures driven by concentrated solar process heat.

H_2O/CO_2-splitting

The single-step thermal dissociation of water or CO_2, known as solar thermolysis, although conceptually simple, has been impeded by the need to operate at above 2500 K for achieving a reasonable degree of dissociation, and by the need of an

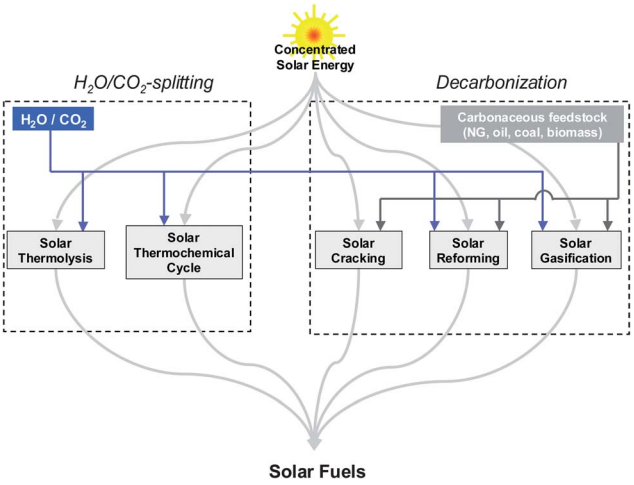

Fig. 8 Thermochemical routes for solar fuel production using concentrated solar radiation as the energy source of high-temperature process heat. Indicated is the chemical feedstock: H_2O/CO_2 and/or carbonaceous feedstock (*e.g.* natural gas, oil, coal, and biomass). Based on the feedstock, the processes are grouped into H_2O/CO_2-splitting processes (solar thermolysis and solar thermochemical cycles) and decarbonization processes (solar cracking, solar reforming, and solar gasification).

effective technique for separating H_2 and O_2 or CO and O_2 at high temperatures to avoid ending up with an explosive mixture. Among the ideas investigated were solar-heated zirconia membranes and other ceramic materials, followed by effusion or electrolytic separation.[64,66–68] Water-splitting thermochemical cycles bypass the H_2/O_2 separation problem and further allow operating at relatively moderate upper temperatures. Previous studies performed on H_2O-splitting thermochemical cycles were mostly characterized by the use of process heat at temperatures below about 1000 K, available from nuclear and other thermal sources. These cycles required multiple steps (>2) and suffered from inherent inefficiencies associated with heat transfer and product separation at each step. In recent years, significant progress has been accomplished in the development of CSP systems capable of achieving $C > 5000$. Such high solar radiation fluxes allow the conversion of solar energy to thermal reservoirs at 1500 K and above which are needed for the more efficient two-step thermochemical cycles using metal oxide redox reactions.[65,69–73] The H_2O/CO_2-splitting redox cycle can be represented by:

1st step, reduction

$$MO_{ox} \rightarrow MO_{red} + \frac{1}{2} O_2 \quad (5)$$

2nd step, oxidation

$$MO_{red} + H_2O \rightarrow MO_{ox} + H_2 \quad (6)$$

$$MO_{red} + CO_2 \rightarrow MO_{ox} + CO \quad (7)$$

The first, endothermic step is the solar thermal reduction of the metal oxide MO_{ox} to the metal or the lower-valence metal oxide MO_{red}. The second, non-solar, exothermic step is the reaction of the reduced metal oxide with H_2O or CO_2 to form H_2 or CO, and reform the original metal oxide which is recycled to the first step. The net reactions are $H_2O = H_2 + 0.5O_2$ and $CO_2 = CO + 0.5O_2$, but since H_2/CO and O_2 are formed in different steps, the need for high-temperature gas separation is thereby eliminated. The second step can be accomplished on demand at the fuel consumer site, as it is decoupled from the availability of solar energy. CO_2 and H_2O can be co-fed to produce synthesis gas (syngas), the building block for a wide variety of synthetic fuels including Fischer–Tropsch liquid hydrocarbon fuels. Amongst candidate redox materials, ferrite-based and analogous "non-volatile" oxides exhibit relatively slow reaction rates, degradation in rates due to sintering, and losses due to uncontrolled sublimation, whereas ZnO, SnO_2, and analogous "volatile" oxides that sublime during decomposition require rapid quenching of gaseous products to avoid recombination.

One promising redox system is ZnO/Zn, for which the theoretical maximum $\eta_{solar\text{-}to\text{-}fuel} = 35$–$50\%$ depending on the level of heat recovery during quenching and hydrolysis.[74–77] The ZnO-dissociation proceeds at reasonable rates at above 1700 °C while the products Zn(g) and O_2 need to be quenched or separated at high temperatures to avoid their recombination.[78,79] Various solar reactor concepts were examined experimentally, including entrained flows,[80] packed beds,[81] and rotating cavity-receivers.[82,83] Fig. 9a shows a solar chemical reactor configuration for performing the thermal dissociation of ZnO that consists of a windowed rotating cavity-receiver lined with ZnO particles.[84] With this arrangement, ZnO is directly exposed to high-flux solar irradiation and serves simultaneously the functions of radiant absorber, thermal insulator, and chemical reactant. For $Q_{solar} = 11$ kW, the experimental measured $\eta_{solar\text{-}to\text{-}fuel}$ was 3.1% (based on the HV of the zinc produced).[83] The second step of the cycle, eqn (6) and (7), has been demonstrated using an aerosol flow reactor for *in situ* formation and hydrolysis of Zn nanoparticles,[85–90] as well as for CO_2 reduction with Zn nanoparticles.[91] The high specific surface area of nanoparticles leads to high Zn-to-ZnO conversions over short residence times due to augmented reaction kinetics and heat/mass transfer. However, the reactions primarily occurred heterogeneously on reactor wall surfaces. The kinetics of the reaction of Zn with CO_2 and mixtures of H_2O and CO_2, studied by thermogravimetry,[92–94] exhibited an initial fast interface-controlled regime that transitioned to a slower diffusion-controlled regime limited by ion mobility through the ZnO layer. Laboratory studies were performed with steam bubbling through molten zinc,[95] but the continuous removal of ZnO(s) may pose process complications. Analogous to the ZnO/Zn redox system, the volatile SnO_2–SnO pair is characterized by the formation SnO in the vapor phase during the solar step.[96]

A non-volatile redox system extensively investigated is the Fe_3O_4/FeO,[76,77,92–99] which requires upper operating temperatures similar to those for the ZnO/Zn system but without undergoing sublimation. For CO_2-splitting, $\eta_{solar\text{-}to\text{-}fuel} = 29\%$ (no sensible heat recovery between cycles) because of the higher solar energy input required and higher heat loss by quenching per mole of CO_2 reduced.[77] Spinel ferrites of the form $M_xFe_{3-x}O_4$, where M generally represents Ni, Zn, Co, Mn, or other transition metals, have been shown to be capable of splitting water at moderate and more workable upper operating temperatures.[100–106] The drawbacks are associated with the need to provide an inert gas or vacuum pressures to drive the metal oxide

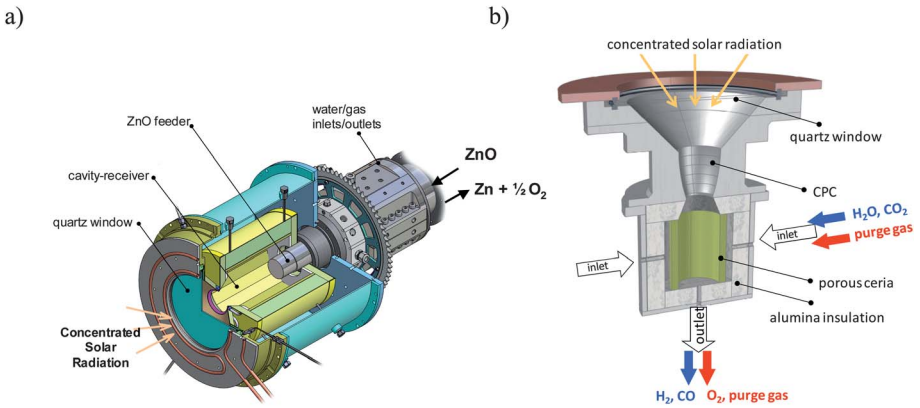

Fig. 9 (a) Scheme of the solar reactor for the Zn/ZnO redox cycle.[84] It consists of windowed cavity-receiver lined with ZnO particles and directly exposed to high-flux solar irradiation. (b) Scheme of the solar reactor for the CeO_2–$CeO_{2-\delta}$ redox cycle.[115] It consists of a windowed cavity-receiver containing a porous monolithic ceria subjected to multiple heat–cool cycles under appropriate gases to induce fuel production. Red arrow indicates ceria reduction (oxygen evolution); blue arrow indicates oxidation (fuel production).

reduction, which translates into an energy penalty, as well as the relatively small fraction of oxygen per unit weight of metal oxide liberated during the reduction, which introduces scale-up limitations and imposes the need to recover sensible heat between cycles for achieving acceptable $\eta_{\text{solar-to-fuel}}$. The solar reactor concepts tested include ferrite-coated monoliths,[107,108] circulating fluidized beds,[109] and rotating disks.[110,111] The latter design concept utilizes two sets of beds of ferrite reactant materials in close proximity and rotating in opposite directions for thermal recuperation.

Ceria-based oxides have emerged as attractive non-volatile redox candidates because they display faster kinetics and better stability and selectivity relative to the ferrite-based oxides.[112–114] Fig. 9b shows a solar chemical reactor configuration for performing both steps of the CeO_2–$CeO_{2-\delta}$ cycle.[115] The simultaneous splitting of H_2O and CO_2 was experimentally shown in 10 consecutive cycles, yielding syngas with a H_2 : CO molar ratio that can be controlled by adjusting the H_2O : CO_2 molar ratio in the reacting gas.[116] A H_2 : CO molar ratio in the range 1.7–2 would be suitable for the processing to liquid hydrocarbon fuels (*e.g.* diesel, kerosene) *via* Fischer–Tropsch synthesis. For $Q_{\text{solar}} =$ 3 kW, the experimental measured $\eta_{\text{solar-to-fuel}}$ was 0.8% (based on the HHV of the fuel produced), but no attempt was undertaken to optimize the system for maximum efficiency.[115] Both the efficiency and the cycling rates in the reactor were limited largely by thermal losses resulting from conductive and radiative heat transfer. A thermodynamic analysis indicates the potential of reaching $\eta_{\text{solar-to-fuel}} = 20\%$ in the absence of heat recovery, and exceeding 30% by recovering the sensible heat of the hot products.[117]

An alternative path to solar fuels from H_2O and CO_2 is the electrolysis, provided electricity is generated by solar energy. The current density of alkaline cells is typically around 0.3–0.4 A cm^{-2}, with cell efficiencies in the 52–70% range based on the HHV of H_2.[118] These values will have to be multiplied by the efficiency of solar power generation to obtain $\eta_{\text{solar-to-fuel}}$. Some of the R&D challenges include development of new diaphragm/membrane materials of controlled porosity and mechanical strength, and improvement of stack materials and components to increase reliability, durability, and efficiency by reducing cell voltage and resistance of the cell assembly. High-temperature steam electrolysis offers the possibility of using concentrated solar heat to reduce the electric energy input.[119] Solid oxide cells are operated in the range of 800–1000 °C but the formation of secondary isolating phases at the triple phase and electrolyte–electrode boundaries has a detrimental effect on stability and efficiency. The main challenges are the development of chemically stable and gastight electrolytes with high ionic and low electronic conductivity, and of chemically stable electrodes in highly reducing–oxidizing environments with good electronic conduction. Co-electrolyzing H_2O and CO_2 results in lower cell resistance, with estimated 70% cell efficiency and overall $\eta_{\text{solar-to-fuel}} \approx 10\%$.[120,121] With photocatalytic approaches, $\eta_{\text{solar-to-fuel}}$ is currently about two orders of magnitude lower.[122]

Decarbonization

The solar cracking route refers to the thermal decomposition of natural gas (NG), oil, and other hydrocarbons, and can be represented by the simplified net reaction:

$$C_xH_y = xC(\text{gr}) + \frac{y}{2}H_2 \quad (8)$$

Other compounds may also be formed, depending on the presence of impurities in the raw materials. The thermal decomposition yields a carbon-rich condensed phase and a hydrogen-rich gas phase. The carbonaceous solid product can either be sequestered without CO_2 release or used as a material commodity under less severe CO_2 restraints. It can also be applied as a reducing agent in metallurgical processes. From the point of view of carbon sequestration, it is easier to separate, handle, transport, and store solid carbon than gaseous CO_2. Assuming carbon sequestration, eqn (4) yields a theoretically maximum $\eta_{\text{solar-to-fuel}} = 0.55$.[123] Solar reactor concepts proposed for this process include directly irradiated particle flows[124,125] and indirectly irradiated graphite/ceramic absorber tubes.[126–128] Fig. 10a shows a scheme of a solar reactor that features a continuous flow of CH_4 laden with μm sized carbon black particles, confined to a cavity receiver and directly exposed to concentrated solar irradiation. The laden carbon particles serve

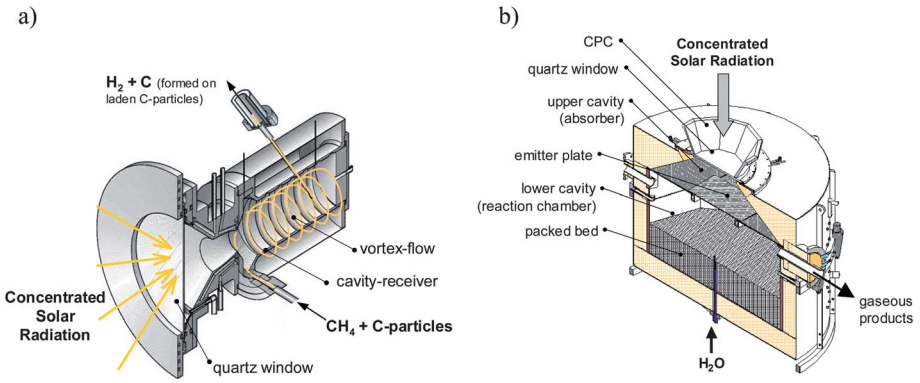

Fig. 10 (a) Scheme of the solar reactor for the co-production C and H_2 by thermal decomposition of CH_4. It consists of a continuous flow of CH_4 laden with μm sized carbon black particles, confined to a windowed cavity-receiver and directly exposed to concentrated solar irradiation.[124] (b) Scheme of the solar reactor for the production of syngas by thermal gasification of carbonaceous feedstock. It consists of two cavities in series, with the upper one serving as the solar absorber and the lower one containing a reacting packed-bed.[133]

the functions of radiant absorbers and nucleation sites for the heterogeneous reaction.[124]

The steam-reforming of hydrocarbons (*e.g.* NG, oil, and others), and the steam-gasification of carbonaceous materials (*e.g.* coal, coke, biomass, and other C-containing solids) can be represented by the simplified net reaction:

$$C_xH_yO_z + (x - z)H_2O = \left(\frac{y}{2} + x - z\right)\cdot H_2 + xCO \qquad (9)$$

Other compounds may also be formed (*e.g.* H_2S), depending on the impurities contained in the feedstock. The principal product is high-quality syngas. For example, the solar steam-based gasification of anthracite coal at above 1500 K yields syngas with a H_2 : CO molar ratio of 1.2 and a CO_2 : CO molar ratio of 0.01. In contrast, the conventional (non-solar) gasification process is carried out autothermally, *i.e.* by combusting at least one-third of the feedstock internally to generate the required process heat. The advantages of the solar-driven process *vis-à-vis* the conventional autothermal process are 5-fold: (1) it delivers higher syngas output per unit of feedstock, as no portion of the feedstock is combusted for process heat; (2) it avoids contamination of syngas with combustion byproducts, and consequently reduces costly downstream gas cleaning and separation requirements; (3) it produces syngas with higher calorific value and lower CO_2 intensity, as the energy content of the feedstock is upgraded up to 33% through the solar energy input; (4) it allows for higher gasification temperatures (above 1200 °C), resulting in faster reaction kinetics and higher quality of the syngas produced with low or without tar content; and (5) it eliminates the need for an upstream air separation unit, as steam is the only gasifying agent, which further facilitates economic competitiveness.

For the solar steam-reforming of NG and the steam-gasification of coal followed by syngas processing to H_2 (assuming water–gas shift and H_2/CO_2 separation unit based on the pressure swing adsorption technique at 90% recovery rate), eqn (4) yields a theoretically maximum $\eta_{\text{solar-to-fuel}} = 0.71$.[123] A solar reactor for the solar reforming of NG that uses a reticulate porous ceramic foam coated with Rh-based catalyst has been scaled up to power levels of 300 kW in a solar tower facility.[129] The solar steam-gasification of various carbonaceous feedstocks, *e.g.* coal, petroleum coke, biochar, and waste carbon-containing materials, was studied in fluidized-bed, entrained-flow, and packed-bed solar reactors.[130–133] Fig. 10b shows a scheme of a packed-bed solar reactor that features two cavities in series.[133] The upper cavity functions as the solar absorber and contains a windowed aperture to let in concentrated solar radiation. The lower cavity functions as the reaction chamber and contains a packed-bed of solid carbonaceous feedstock on top of the steam injector. This design accepts bulk carbonaceous feedstock without prior processing of any shape and size, and uses the moisture content in feedstock for steam-based gasification. The reactor is operated in batch mode, typically 1 batch per day adapted to the availability of the sun, with the packed bed shrinking as the gasification progresses. If biomass is used as feedstock, the syngas produced is CO_2-neutral. A recent review of solar reactor technologies for the solar-driven gasification of carbonaceous feedstock is given in ref. 134.

7. Summary and conclusions

After three decades of R&D, the industrial implementation of CSP systems is rapidly increasing. Current technologies are based on solar receivers that operate with thermal oil, molten salts or water–steam at working temperatures usually below 600 °C, coupled to steam-based Rankine cycles for power generation at 20% peak efficiency. The next generation of technologies allows surpassing 1000 °C and enables higher efficiencies *via* Brayton–Rankine combined cycles, as well as better integration of thermal storage and hybridization with fossil-fuel backup. Novel receiver concepts based on volumetric absorption of directly irradiated porous structures, particles, and alternative thermal fluids operate at high temperatures/high fluxes and promise more efficient solar energy capture and conversions. Moreover, these advance concepts can be applied for the thermochemical production of solar fuels. Solar cracking, reforming, and gasification processes for upgrading and converting carbonaceous feedstock to syngas conserve fossil fuels, reduce emissions, and could become an important transition path towards solar fuels. The production of solar hydrogen, syngas, and liquid hydrocarbon fuels from H_2O and CO_2 *via* 2-step redox cycles has favorable long-term potential, warranting further development and large-scale demonstration.

Nomenclature

C	Solar flux concentration ratio
I	Direct normal solar irradiation (DNI)
$\dot{n}$	Molar flow rate
HHV	High heating value
Q_{solar}	Solar energy coming from the solar concentrator
T	Nominal solar reactor temperature
$T_{stagnation}$	Maximum temperature of a blackbody absorber
$T_{optimum}$	Optimal temperature of the solar reactor for maximum
ΔG	Gibbs free energy change
ΔH	Enthalpy change
$\eta_{absorption}$	Solar energy absorption efficiency
η_{Carnot}	Efficiency of a Carnot heat engine operating between T_H and T_L
$\eta_{solar\text{-}to\text{-}fuel}$	Solar-to-fuel energy conversion efficiency
σ	Stefan–Boltzmann constant (5.6705×10^{-8} Wm^{-2} K^{-4})
θ_S	Semi-angle subtended by the sun
ϕ_{rim}	CPC acceptance angle
ϕ_{CPC}	Parabolic rim angle.

References

1 A. Pifre, *Nature*, 1882, **21**, 503–504.
2 J. Ericsson, *Nature*, 1888, **38**, 321.
3 A. Eneas, *US Pat.*, 670,917, 1901.
4 F. Shuman, *Sci. Am.*, 1913, **109**, 350.
5 G. Francia, *Sol. Energy*, 1968, **12**, 51–64.
6 *Solar Power Plants*, ed. C. J. Winter, R. L. Sizmann and L. L. Vant-Hull, Springer-Verlag, Berlin, 1991.
7 M. Romero and E. Zarza, in *Handboook of Energy Efficiency and Renewable Energy*, ed. F. Kreith and Y. Goswami, CRC Press Taylor & Francis Group, Boca Raton, Florida, 2007, ch. 21, pp. 1–98.
8 M. Becker, W. Meinecke, M. Geyer, F. Trieb, M. Blanco, M. Romero and A. Ferriere, in *The Future for Renewable Energy 2: Prospects and Directions*, Eurec Agency. Pub. James & James Science Publishers Ltd., London, UK, 2002, pp. 115–137.
9 A. Rabl, *Active Solar Collectors and Their Applications*, Oxford University Press, New York, 1985, pp. 59–66.
10 Y. Goswami, F. Kreith and J. F. Kreider, *Principles of Solar Engineering*, Taylor & Francis Group, New York, 2nd edn, 2000.
11 W. T. Welford and R. Winston, *High Collection Nonimaging Optics*, Academic Press, San Diego, 1989.
12 M. Romero and J. González Aguilar, *Energy & Power Generation Handbook*, ed. K. R. Rao, ASME Three Park Avenue, New York, NY 10016-5990, USA, 2011, ch. 3.
13 D. Mills, *Sol. Energy*, 2004, **76**, 19–31.
14 A. Yogev, A. Kribus, M. Epstein and A. Kogan, *Int. J. Hydrogen Energy*, 1998, **23**, 239–245.
15 T. Mancini, P. Heller, B. Butler, B. Osborn, W. Schiel, V. Goldberg, R. Buck, R. Diver, C. Andraka and J. Moreno, *J. Sol. Energy Eng.*, 2003, **125**, 135–151.
16 C. Lopez and K. Stone, *Proc. of ASME Int. Solar Energy Conf.*, Maui, HI, ISBN 0-7918-762-2, 1992, pp. 945–952.
17 T. Keck, P. Heller and G. Weinrebe, *Proc. ISES Solar World Congress*, Göteborg, Sweden, June 2003.
18 W. Stine and R. B. Diver, report SAND93-7026, Sandia National Laboratories, Albuquerque, New Mexico, 1994.
19 A. T. Kearney, *Solar thermal electricity 2025, STE industry roadmap for the European Solar Thermal Electricity Association (ESTELA)*, 2010, www.atkearney.com.
20 G. Herring, *Concentrating solar thermal power gains steam in Spain, as momentum builds for major projects in the US, North Africa, the Middle East, Asia and Australia*, Photon International, December 2009, pp. 46–52.
21 IEA, *Energy Technology Perspectives 2010 – Scenarios and Strategies to 2050*, 2010, ISBN 978-92-64-08597-8.
22 IEA, *Technology Roadmap – Concentrating Solar Power*, 2010, http://www.iea.org.
23 R. Pitz-Paal, J. Dersch, B. Milow, A. Ferriere, M. Romero, F. Téllez, E. Zarza, A. Steinfeld, U. Langnickel, E. Shpilrain, O. Popel, M. Epstein and J. Karni, *ECOSTAR Roadmap Document for the European Commission*, ed. Pitz-Paal, Dersch and Milow, Deutsches Zentrum für Luft- und Raumfahrt e.V., SES-CT-2003–502578, Cologne, Germany, February 2005, http://www.vgb.org/data/vgborg_/Forschung/roadmap252.pdf.
24 R. Bader, A. Pedretti and A. Steinfeld, *ASME J. Sol. Energy Eng.*, 2012, **134**, 021002–021011.
25 M. Haenchen, S. Brückner and A. Steinfeld, *Appl. Therm. Eng.*, 2011, **31**, 1798–1806.
26 M. Zebarjadi, K. Esfarjani, M. S. Dresselhaus, Z. F. Ren and G. Chen, *Energy Environ. Sci.*, 2012, **5**, 5147–5162.
27 Y. G. Deng and J. Liu, *J. Renewable Sustainable Energy*, 2009, **1**, 052701.
28 D. Kraemer, B. Poudel, H. P. Feng, J. C. Caylor, B. Yu, X. Yan, Y. Ma, X. Wang, D. Wang, A. Muto, K. McEnaney, M. Chiesa, Z. Ren and G. Chen, *Nat. Mater.*, 2010, **9**, 762–767; D. Kraemer, B. Poudel, H. P. Feng, J. C. Caylor, B. Yu, X. Yan, Y. Ma, X. Wang, D. Wang, A. Muto, K. McEnaney, M. Chiesa, Z. Ren and G. Chen, *Nat. Mater.*, 2011, **10**, 532–538.
29 C. Suter, P. Tomes, A. Weidenkaff and A. Steinfeld, *Sol. Energy*, 2011, **85**, 1511–1518.
30 M. Romero, M. J. Marcos, F. M. Téllez, M. Blanco, V. Fernández, F. Baonza and S. Berger, *Sol. Energy*, 2000, **67**(4–6), 249–264.
31 G. J. Kolb, *Sol. Energy*, 1998, **62**, 51–61.
32 P. K. Falcone, SAND86-8009, Sandia National Laboratories, Livermore, USA, 1986.
33 W. Grasse, H. P. Hertlein and C. J. Winter, *Solar Power Plants*, ed. C. J. Winter, R. L. Sizmann, L. L. Vant-Hull, Springer-Verlag, Berlin, 1991, pp. 215–282.
34 L. G. Radosevich and A. C. Skinrood, *J. Sol. Energy Eng.*, 1989, **111**, 144–151.
35 J. E. Pacheco and R. Gilbert, in *Renewable and Advanced Energy Systems for the 21st Century RAES'99 April 11–15, 1999*, ed. R. Hogan, Y. Kim, S. Kleis, D. O'Neal and T. Tanaka, ASME, Maui, Hawaii, New York, 1999, pp. RAES99-7731.
36 J. Lata, S. Alcalde, D. Fernández, X. Lekube, I. Agarraberes, E. Martínez, J. Olano and I. Eguidazu, *Proceedings of International Symposium on Concentrating Solar Power and Chemical Energy Systems. September 20–23, 2011, Granada, Spain*,ed. C I E M A T. Ref. manuscript: 39417, SolarPACES, Spain, 2011.
37 J. I. Burgaleta, S. Arias and I. B. Salbidegoitia, *Proceedings SolarPACES 2009 (CD), Berlin, Germany; 15–18 September 2009*, ed. D L R, Stuttgart, Germany, Ref. Manuscript: 11720, 2009.
38 M. Sánchez and M. Romero, *Sol. Energy*, 2006, **80**, 861–874.
39 C. J. Noone, M. Torrilhon and A. Mitsos, *Sol. Energy*, 2012, **86**, 792–803.
40 F. W. Lipps and L. L. Vant-Hull, *Sol. Energy*, 1978, **20**, 505–516.
41 B. L. Kistler, Sandia report, SAND-86–8018, Sandia National Laboratories, USA, 1986.
42 C. L. Mavis, Sandia Report SAND87–8025, Sandia Nat. Labs., USA, 1989.
43 M. Romero, E. Conejero and M. Sánchez, *Sol. Energy Mater.*, 1991, **24**, 320–332.
44 R. Monterreal, M. Romero, G. García and G. Barrera, in *Solar Engineering 1997*, ed. D. E. Claridge and J. E. Pacheco, ASME, New York, 1997, pp. 251–259.
45 R. Osuna, V. Fernández, M. Romero and M. Sanchez, *Proceedings 12th SolarPACES International Symposium, 6–8 October 2004, Oaxaca, Mexico*, ed. C. Ramos and J. Huacuz, S3-102. CD-Rom, México, 2004.
46 G. J. Kolb, S. A. Jones, M. W. Donnelly, D. Gorman, R. Thomas, R. Davenport and R. Lumia, *Heliostat Cost Reduction Study*, SANDIA Report SAND2007–3293, 2007.

47 E. Silberstein, Y. Magen, G. Kroyzer, R. Hayut and H. Huss, *Proceedings SolarPACES 2009 (CD). Berlín, Germany; 15–18 September 2009*. ed. D L R, Stuttgart, Germany, 2009.
48 S. Schell, *Proceedings SolarPACES 2009 (CD). Berlín, Germany; 15–18 September 2009*. ed. D L R, Stuttgart, Germany, 2009.
49 M. Romero, R. Buck and J. E. Pacheco, *J. Sol. Energy Eng.*, 2002, **124**, 98–108.
50 M. Becker and L. L. Vant-Hull, in *Solar Power Plants*, ed. C. J. Winter, R. L. Sizmann and L. L. Vant-Hull, Springer-Verlag, Berlin, 1991, pp. 163–197.
51 A. L. Avila-Marin, *Sol. Energy*, 2011, **85**, 891–910.
52 S. Haussener, P. Coray, W. Lipinski, P. Wyss and A. Steinfeld, *ASME J. Heat Transfer*, 2010, **132**(023305), 1–9.
53 C. Agrafiotis, I. Mavroidis, A. G. Konstandopoulos, B. Hoffschmidt, P. Stobbe, M. Romero and V. Fernández-Quero, *Sol. Energy Mater. Sol. Cells*, 2007, **91**, 474–488.
54 J. Petrasch, P. Wyss and A. Steinfeld, *J. Quant. Spectrosc. Radiat. Transfer*, 2007, **105**, 180–197.
55 S. Palero, M. Romero and J. L. Castillo, *J. Sol. Energy Eng.*, 2008, **130**, 011011.
56 M. J. Marcos, M. Romero and S. Palero, *Energy*, 2004, **29**, 677–686.
57 B. Hoffschmidt, V. Fernandez, R. Pitz-Paal, M. Romero, P. Stobbe and F. Téllez, *11th SolarPACES International Symposium on Concentrated Solar Power and Chemical Energy Technologies. September 4-6, 2002., Zurich, Switzerland*, 2002, pp. 117–126.
58 M. Romero, M. J. Marcos, R. Osuna and V. Fernández, *Proceedings of the ASME International Solar Energy Conference, Madison, Wisconsin, June 16–21, 2000*. ed. J. D. Pacheco and M. D. Thornbloom, ASME, New York, 2000.
59 I. Hischier, P. Leumann and A. Steinfeld, *J. Sol. Energy Eng.*, 2012, **134**, 021003–021011.
60 J. Karni, A. Kribus, P. Doron, R. Rubin, A. Fiterman and D. Sagie, *J. Sol. Energy Eng.*, 1997, **119**, 74–78.
61 F. Tellez, M. Romero, P. Heller, A. Valverde, J. F. Reche, S. Ulmer and G. Dibowski, *Proceedings 12th SolarPACES International Symposium, 6–8 October 2004, Oaxaca, Mexico*, ed. C. Ramos and J. Huacuz, S9-206. CD-Rom, México, 2004.
62 A. Kribus, in *Solar Thermal Electricity Generation. Colección Documentos CIEMAT*, CIEMAT, Madrid, Spain, 1999, pp. 251–285, ISBN: 84-7834-353-9.
63 A. Steinfeld and R. Palumbo, in *Encyclopedia of Physical Science & Technology*, ed. R. A. Meyers, Academic Press, 2001, vol. 15, pp. 237–256.
64 E. A. Fletcher and R. L. Moen, *Science*, 1977, **197**, 1050–1056.
65 A. Steinfeld, *Sol. Energy*, 2005, **78**, 603–615.
66 A. Kogan, *Int. J. Hydrogen Energy*, 1998, **23**, 89–98.
67 E. A. Fletcher, *Ind. Eng. Chem. Res.*, 1999, **38**, 2275–2282.
68 A. J. Traynor and R. J. Jensen, *Ind. Eng. Chem. Res.*, 2002, **41**, 1935–1939.
69 C. Perkins and A. W. Weimer, *AIChE J.*, 2009, **55**, 287–293.
70 S. Abanades, P. Charvin, G. Flamant and P. Neveu, *Energy*, 2006, **31**, 2805–2822.
71 T. Kodama, *Prog. Energy Combust. Sci.*, 2003, **29**, 567–597.
72 T. Kodama and N. Gokon, *Chem. Rev.*, 2007, **107**, 4048–4077.
73 R. F. Service, *Science*, 2009, **326**, 1472–1475.
74 A. Steinfeld, *Int. J. Hydrogen Energy*, 2002, **27**, 611–619.
75 C. Perkins and A. W. Weimer, *Int. J. Hydrogen Energy*, 2004, **29**, 1587–1599.
76 P. Charvin, S. Abanades, F. Lemort and G. Flamant, *Energy Convers. Manage.*, 2008, **49**, 1547–1556.
77 M. E. Galvez, P. Loutzenhiser, I. Hischier and A. Steinfeld, *Energy Fuels*, 2008, **22**, 3544–3550.
78 L. Schunk and A. Steinfeld, *AIChE J.*, 2009, **55**, 1497–1504.
79 S. Möller and R. Palumbo, *Chem. Eng. Sci.*, 2001, **56**, 4505–4515.
80 C. Perkins, P. R. Lichty and A. W. Weimer, *Int. J. Hydrogen Energy*, 2008, **33**, 499–510.
81 L. Schunk, W. Lipinski and A. Steinfeld, *AIChE J.*, 2009, **55**, 1659–1666.
82 S. Abanades, P. Charvin and G. Flamant, *Chem. Eng. Sci.*, 2007, **62**, 6323–6333.
83 L. Schunk, W. Lipinski and A. Steinfeld, *Chem. Eng. J.*, 2009, **150**, 502–508.
84 L. Schunk, P. Haeberling, S. Wepf, D. Wuillemin, A. Meier and A. Steinfeld, *J. Sol. Energy Eng.*, 2008, **130**, 021009.
85 R. Weiss, K. Wegener, S. E. Pratsinis and A. Steinfeld, *AIChE J.*, 2005, **51**, 1966–1970.
86 K. Wegner, H. Ly, R. Weiss, S. E. Pratsinis and A. Steinfeld, *Int. J. Hydrogen Energy*, 2005, **31**, 55–61.
87 T. Abu Hamed, J. Davidson and M. Stolzenburg, *J. Sol. Energy Eng.*, 2008, **130**, 041010.
88 H. H. Funke, H. Diaz, X. Liang, C. S. Carney, A. W. Weimer and P. Li, *Int. J. Hydrogen Energy*, 2008, **33**, 1027–1134.
89 F. O. Ernst, A. Tricoli, S. E. Pratsinis and A. Steinfeld, *AIChE J.*, 2006, **52**, 3297–3303.
90 T. Melchior, N. Piatkowski and A. Steinfeld, *Chem. Eng. Sci.*, 2009, **64**, 1095–1101.
91 P. Loutzenhiser, E. Galvez, I. Hischier, A. Graf and A. Steinfeld, *Chem. Eng. Sci.*, 2010, **65**, 1855–1864.
92 P. Loutzenhiser, M. E. Galvez, I. Hischier, A. Stamatiou, A. Frei and A. Steinfeld, *Energy Fuels*, 2009, **23**, 2832–2839.
93 A. Stamatiou, P. Loutzenhiser and A. Steinfeld, *Chem. Mater.*, 2010, **22**, 851–859.
94 A. Stamatiou, P. Loutzenhiser and A. Steinfeld, *Energy Fuels*, 2010, **24**, 2716–2722.
95 A. Berman and M. Epstein, *Int. J. Hydrogen Energy*, 2000, **20**, 957–967.
96 S. Abanades, P. Charvin, F. Lemont and G. Flamant, *Int. J. Hydrogen Energy*, 2008, **33**, 6021–6030.
97 A. Steinfeld, S. Sanders and R. Palumbo, *Sol. Energy*, 1999, **65**, 43–53.
98 P. Charvin, S. Abanades, G. Flamant and F. Lemort, *Energy*, 2007, **32**, 1124–1133.
99 K. Ehrensberger, R. Palumbo, C. Larson and A. Steinfeld, *Ind. Eng. Chem. Res.*, 1997, **36**, 645–648.
100 Y. Tamaura, A. Steinfeld, P. Kuhn and K. Ehrensberger, *Energy*, 1995, **20**, 325–330.
101 F. Fernando, R. Fernandez-Saavedra, M. Gomez-Mancebo, A. Vidal, M. Sanchez, M. Rucandio, A. Quejido and M. Romero, *Int. J. Hydrogen Energy*, 2009, **34**, 2918–2924.
102 J. E. Miller, M. D. Allendorf, R. B. Diver, L. R. Evans, N. P. Siegel and J. N. Stuecker, *J. Mater. Sci.*, 2008, **43**, 4714–4728.
103 M. D. Allendorf, R. B. Diver, N. P. Siegel and J. E. Miller, *Energy Fuels*, 2008, **22**, 4115–4124.
104 N. Gokon, H. Murayama, A. Nagasaki and T. Kodama, *Sol. Energy*, 2009, **83**, 527–537.
105 N. Gokon, T. Hasegawa, S. Takahashi and T. Kodama, *Energy*, 2008, **33**, 1407–1416.
106 H. Ishihara, H. Kaneko, N. Hasegawa and Y. Tamaura, *Energy*, 2008, **33**, 1788–1793.
107 C. Agrafiotis, M. Roeb, A. G. Konstandopoulos, L. Nalbandian, V. T. Zaspalis, C. Sattler, P. Stobbe and A. M. Steele, *Sol. Energy*, 2005, **79**, 409–421.
108 M. Roeb, C. Sattler, R. Klueser, N. Monnerie, L. De Oliveira, A. G. Konstandopoulos, C. Agrafiotis, V. Zaspalis, L. Nalbandian, A. Steele and P. Stobbe, *J. Sol. Energy Eng.*, 2006, **128**, 125–133.
109 N. Gokon, S. Takahashi, H. Yamamoto and T. Kodama, *Int. J. Hydrogen Energy*, 2008, **33**, 2189–2199.
110 H. Kaneko, T. Miura, A. Fuse, H. Ishihara, S. Taku, H. Fukuzumi, Y. Naganuma and Y. Tamaura, *Energy Fuels*, 2007, **21**, 2287–2293.
111 R. B. Diver, J. E. Miller, M. D. Allendorf, N. P. Siegel and R. E. Hogan, *J. Sol. Energy Eng.*, 2008, **130**, 041001.
112 W. C. Chueh and S. M. Haile, *ChemSusChem*, 2009, **2**, 735–739.
113 W. C. Chueh and S. M. Haile, *Philos. Trans. R. Soc. London, Ser. A*, 2010, **368**, 3269–3294.
114 S. Abanades, A. Legal, A. Cordier, G. Peraudeau, G. Flamant and A. Julbe, *J. Mater. Sci.*, 2010, **45**, 4163–4173.
115 W. C. Chueh, C. Falter, M. Abbott, D. Scipio, P. Furler, S. M. Haile and A. Steinfeld, *Science*, 2010, **330**, 1797–1801.
116 P. Furler, J. Scheffe and A. Steinfeld, *Energy Environ. Sci.*, 2012, **5**, 6098–6103.
117 J. Scheffe and A. Steinfeld, *Energy Fuels*, 2012, **26**, 1928–1936.
118 K. Zeng and D. Zhang, *Prog. Energy Combust. Sci.*, 2010, **36**, 307–326.
119 M. Ni, M. K. H. Leung and D. Y. C. Leung, *Int. J. Hydrogen Energy*, 2008, **33**, 2337–2354.
120 W. Haije and H. Geerlings, *Environ. Sci. Technol.*, 2011, **45**, 8609–8610.

121 C. Graves, S. D. Ebbesen and M. Mogensen, *Solid State Ionics*, 2011, **192**, 398–403.
122 S. C. Roy, O. K. Varghese, M. Paulose and C. A. Grimes, *ACS Nano*, 2010, **4**, 1259–1278.
123 P. v. Zedtwitz, J. Petrasch, D. Trommer and A. Steinfeld, *Sol. Energy*, 2006, **80**, 1333–1337.
124 G. Maag, G. Zanganeh and A. Steinfeld, *Int. J. Hydrogen Energy*, 2009, **34**, 7676–7685.
125 A. Kogan, M. Kogan and S. Barak, *Int. J. Hydrogen Energy*, 2005, **30**, 35–43.
126 S. Abanades and G. Flamant, *Int. J. Hydrogen Energy*, 2007, **32**, 1508–1515.
127 J. K. Dahl, K. J. Buechler, A. W. Weimer, A. Lewandowski and C. Bingham, *Int. J. Hydrogen Energy*, 2004, **29**, 725–736.
128 S. Rodat, S. Abanades and G. Flamant, *Int. J. Chem. React. Eng.*, 2010, **8**, A25.
129 S. Moeller, R. Buck, R. Tamme, M. Epstein, D. Liebermann, M. Moshe, U. Fisher, A. Rotstein and C. Sugarmen, Solar Production of Syngas for Electricity Generation, SOLASYS Project Test-phase, in, *Proceedings of the 11th SolarPACES Int. Symposium*, ed. A. Steinfeld, Zurich, Switzerland, 2002, vol. 231–237.
130 A. Z'Graggen, P. Haueter, D. Trommer, M. Romero, J. C. Jesus and A. Steinfeld, *Int. J. Hydrogen Energy*, 2006, **31**, 797–811.
131 P. von Zedwitz and A. Steinfeld, *Ind. Eng. Chem. Res.*, 2005, **44**, 3852–3861.
132 T. Melchior, C. Perkins, P. Lichty, A. W. Weimer and A. Steinfeld, *Chem. Eng. Process.*, 2009, **48**, 1279–1287.
133 N. Piatkowski, C. Wieckert and A. Steinfeld, *Fuel Process. Technol.*, 2009, **90**, 360–366.
134 N. Piatkowski, C. Wieckert, A. Weimer and A. Steinfeld, *Energy Environ. Sci.*, 2011, **4**, 73–82.